applied sciences

MDPI

Article

Analysis of Shield Tunnel Ground Deformation Characteristics and Affecting Factors in Water-Rich Soft Stratum: A Case Study on the Section Tunnel of Tianjin Metro Line 6

Xinyu Li [1,*], Dingli Zhang [2,*] and Yanjuan Hou [2]

[1] State Key Laboratory of Hydroscience and Engineering, Department of Hydraulic Engineering, Tsinghua University, Beijing 100084, China
[2] Key Laboratory of Urban Underground Engineering of Ministry of Education, Beijing Jiaotong University, Beijing 100044, China; yjhou@bjtu.edu.cn
* Correspondence: lixinyu352@mail.tsinghua.edu.cn (X.L.); dlzhang@bjtu.edu.cn (D.Z.); Tel.: +86-152-1058-4045 (X.L.)

Abstract: With the increasing intensity of underground development, the planned metro lines will inevitably pass through water-rich soft stratum. The existing research results show that shield tunneling in water-rich stratum is prone to ground settlement and segment cracking due to the large moisture content and the low soil strength, which will pose risks to the safety of construction. The prediction of ground deformation characteristics and influencing ranges caused by shield tunneling in water-rich soft stratum has been a topical issue among the tunnel research community. Based on the shield tunnel project of Tianjin Metro Line 6, supported by the monitoring data, this paper analyses the ground deformation characteristics caused by shield tunneling in water-rich soft stratum. The results suggest that the surface settlement ranges from −14.20 mm to −28.00 mm in Tianjin's water-rich soft stratum, which is at an acceptable level of engineering. A refined 3D model addressing fluid–structure interactions is developed to consider the construction process in water-rich soft stratum. Based on this technique, this article focuses on the effect of the support pressure at the excavation surface, the friction between the shield skin and the soil, and synchronous grouting quantity on the ground settlement and structural deformation. The results show that the friction between the shield skin and the soil is the most detrimental to deformation control, whereas the synchronous grouting quantity is the most advantageous to ground and segment deformation control. In practice, timely injection of bentonite slurry reduces friction between the shield skin and the soil, and effective synchronous grouting reduces shield tunneling disruption. This technique can provide calculation support in the optimization of shield tunneling schemes in water-rich soft stratum.

Keywords: water-rich soft stratum; shield tunneling; ground deformation; fluid-structure interactions; support pressure at the excavation face; friction between the shield skin and the soil; synchronous grouting quantity

Citation: Li, X.; Zhang, D.; Hou, Y. Analysis of Shield Tunnel Ground Deformation Characteristics and Affecting Factors in Water-Rich Soft Stratum: A Case Study on the Section Tunnel of Tianjin Metro Line 6. *Appl. Sci.* **2022**, *12*, 6208. https://doi.org/10.3390/app12126208

Academic Editor: Daniel Dias

Received: 22 May 2022
Accepted: 16 June 2022
Published: 18 June 2022

1. Introduction

With the acceleration of urbanization, problems of traffic congestion and urban land shortages are becoming increasingly serious [1,2]. Therefore, underground traffic development has become an important way for large and medium-sized cities to relieve traffic congestion [3,4]. The shield tunneling method has gradually become mainstream due to its high automation, safety, ground adaptability, and low impact on the environment in metro construction [5,6]. However, metro construction inevitably produces ground movement, which may cause a negative impact on the nearby surface and subsurface structures in urban areas, and even lead to security incidents. Metro construction in coastal cities faces higher security risks than in other areas. Major security accidents have occurred in Shanghai, Tianjin, Nanjing, Wuhan, Nanning, and Foshan (Figure 1 [7]). For example, the

water inrush and mud gushing in Wuhan Metro Line 3 claimed two lives and injured five people, with direct economic losses worth close to 30 million yuan. In addition, with the increasing intensity of underground development, the planned metro lines will inevitably go below the groundwater level in the future. This situation demonstrates that the safety of shield tunneling in water-rich stratum has become a key problem restricting urban metro construction. Therefore, proper modelling of the ground deformation characteristics because of shield tunneling in water-rich soft stratum is critical. Numerous research works based on empirical formulas, theoretical predictions, model tests, and numerical analyses have been conducted to study the ground settlement caused by shield tunneling.

Figure 1. Safety incidents caused by water [7]. (**a**) Shanghai Metro Line 4 (2003). (**b**) Nanjing Metro Line 2 (2007). (**c**) Tianjin Metro Line 3 (2009). (**d**) Wuhan Metro Line 3 (2013). (**e**) Nanning Metro Line 1 (2014). (**f**) Foshan Metro Line 2 (2018).

Peck [8] proposed a calculation formula to predict surface settlement by analyzing a large number of measured data. Many studies have adapted Peck's formula to fit different geological conditions [9–11], but there are relatively few site-measured data analyses on the ground settlement of shield tunneling in water-rich soft stratum. Furthermore, numerous theoretical analyses have been employed to examine the ground settlement caused by shield tunneling [12]. Based on elastic theory, Sagaseta et al. [13] presented analytic solutions for the strain field due to near-surface ground loss. Loganathan et al. [14] developed a closed form solution used to assess the displacement field around the tunnel. Based on elastic–plastic theory, Pinto et al. [15] put forward analytical solutions for estimating ground movements caused by shallow tunneling in soft ground. Due to the inherent complexities of the ground conditions, the ground settlements obtained by these methods are only suitable for specific conditions. The ground settlement caused by shield tunneling can also be simulated and predicted by the centrifuge model test [16–18]. However, because of its high cost and restricted applicability, the development of this method is limited. Numerical investigation is the most commonly used method in the study of ground responses to shield tunneling [19]. Several numerical models were proposed to simulate the complete construction process. Kasper et al. [20,21] proposed a three-dimensional finite element model for simulations of shield-driven tunnels in soft stratum. The model was used for systematic numerical studies in mechanized tunneling. The model improved the overall behavior of the simulation, but it was still incapable of capturing the real shield movement. Nagel et al. [22,23] investigated the effect of mechanical and hydraulic boundary conditions on pore water pressure at the tunnel face with and without filter cake formation. Jiang et al. [24] developed a three-dimensional finite element model

considering shield conicity and construction process. Zheng et al. [25] proposed a finite element model to investigate the effect of the mechanical driving parameters on ground deformation. From the literature reviews, it can be seen that the prediction of tunneling induced ground deformation by the refined simulation is a very topical issue. Current studies focus on refined simulations in non-water stratum, and less research has been conducted on water-rich soft stratum.

Based on the shield tunnel project of Tianjin Metro Line 6, this paper mainly analyses the ground deformation characteristics caused by shield tunneling in water-rich soft stratum and proposes a refined numerical simulation method addressing fluid–structure interactions. To simulate the friction between the shield skin and the soil, the constant node velocity was applied to the shield shell elements. In addition, the flux boundary was applied to the equivalent zone element to simulate the synchronous grouting process. With this technique, this paper focuses on the influence of key construction parameters such as support pressure on the excavation face, friction between shield skin and soil, and synchronous grouting quantity on ground settlement and structural deformation. This research can provide a calculation basis for shield tunneling decision-making in water-rich soft stratum.

2. Project Overview

The stratum in the Tianjin region is mainly silty clay, silt, and silty sand, with a complicated hydraulic connection. The phreatic aquifer is composed of a filling soil layer, the first marine layer, and the first continental layer, where the elevation of water is approximately −0.5 m. The second continental layer, as well as silt and silty sand from the third continental layer, make up the restricted aquifer, where the elevation of water is about −0.1 m. The section of the Tianjin Metro Line 6 from Hongqinanlu Station to Yingfengdao Station is arranged in a straight line along Hongqi Road, with distinct sections for left and right lines. According to geological exploration reports, we draw the geological section shown in Figure 2. The tunnel passes through a silty clay stratum, which is part of a water-rich soft stratum. It is prone to result in excessive ground deformation. Twelve monitoring sections were arranged along the section tunnel to assure safety, as indicated in Figure 3.

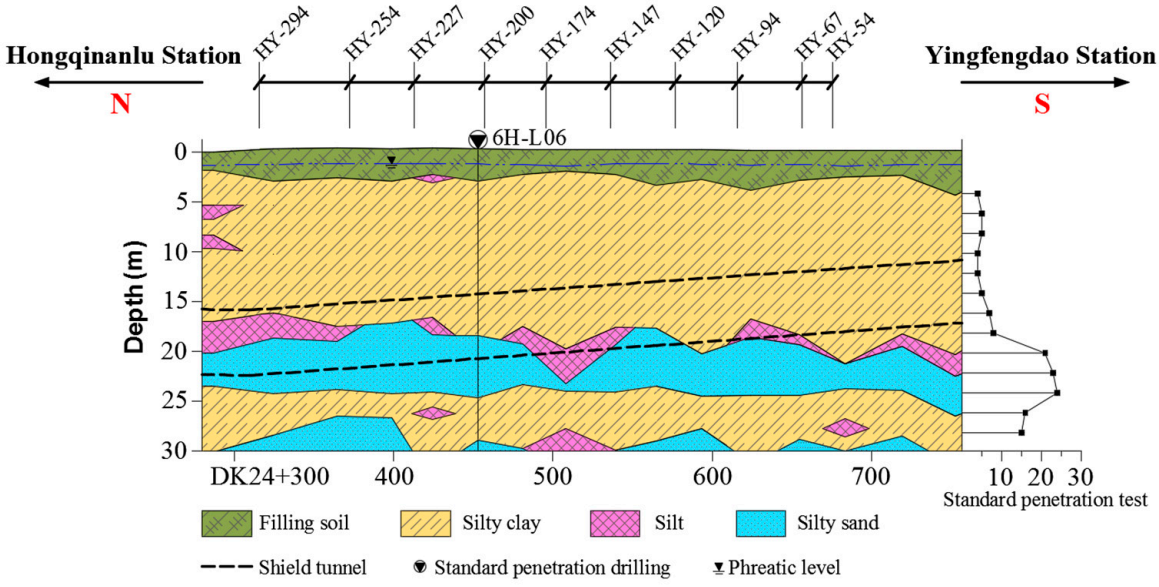

Figure 2. Geological section of the section tunnel.

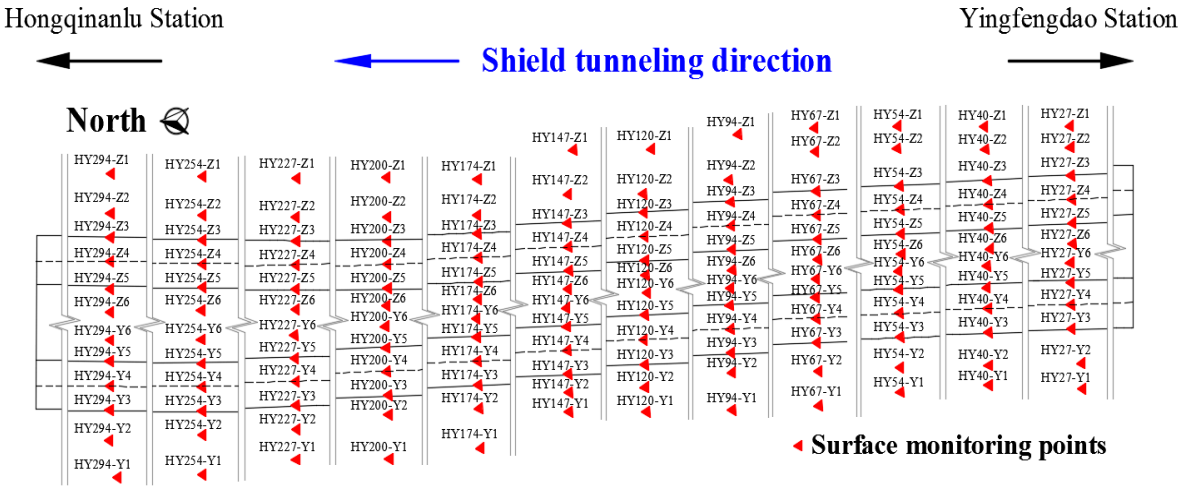

Figure 3. Layout of monitoring sections.

3. Analysis of Ground Deformation Characteristics in Water-Rich Soft Stratum

According to the investigations of Peck et al. [8,26], the surface settlement trough resulting from the single shield tunnel can be illustrated by the Gaussian curve:

$$S(x) = \frac{AV_L}{Kz_0\sqrt{2\pi}} \exp\left(-\frac{x^2}{2(Kz_0)^2}\right) \quad (1)$$

where $S(x)$ is the surface settlement at x from the tunnel centerline; V_L is the ground loss ratio; K is the settlement trough width coefficient; z_0 is the buried depth of the tunnel axis.

The surface settlement produced by the first tunnel construction and the additional surface settlement generated by the second tunnel construction are fitted using the Peck formula, and the two fitting curves are superimposed to obtain the double-line tunnel's surface settlement curve. Table 1 shows the settlement fitting results of the measuring point settlement data for each monitoring section.

Table 1. Settlement trough fitting results of monitoring sections.

Monitoring Section	Stratum	z_0/m	d/m	S_{max}/mm	V_{L1}	V_{L2}	K_1	K_2	$Adj.R_1^2$	$Adj.R_2^2$
HY-027	Homogeneous	14.56	13.30	−17.66	0.82	0.55	0.44	0.48	0.98	0.88
HY-040	Homogeneous	14.83	13.07	−14.20	0.54	0.75	0.45	0.51	0.99	0.99
HY-054	Homogeneous	15.07	13.00	−18.80	0.91	0.54	0.46	0.48	0.99	0.95
HY-067	Homogeneous	15.28	13.00	−15.10	0.77	0.38	0.49	0.53	0.97	0.92
HY-094	Homogeneous	15.76	13.00	−16.00	0.54	0.80	0.48	0.49	0.99	0.95
HY-120	Upper-Soft Lower-Hard	16.24	13.00	−28.00	1.20	0.75	0.41	0.46	0.97	0.90
HY-147	Upper-Soft Lower-Hard	16.66	13.00	−23.10	0.82	1.28	0.37	0.48	0.94	0.90
HY-174	Upper-Soft Lower-Hard	17.05	13.02	−26.90	0.65	1.54	0.30	0.46	0.97	0.80
HY-200	Upper-Soft Lower-Hard	17.59	13.46	−23.70	0.69	1.29	0.33	0.47	0.87	0.97
HY-227	Upper-Soft Lower-Hard	18.19	14.69	−22.45	0.65	1.52	0.30	0.46	0.98	0.90
HY-254	Upper-Soft Lower-Hard	18.67	15.56	−26.4	0.87	1.67	0.35	0.45	0.96	0.86
HY-294	Upper-Soft Lower-Hard	19.18	15.70	−16.50	0.86	0.62	0.37	0.43	0.97	0.71

Where d is the center distance of the double-line tunnel; $S_{\max}$ is the maximum surface settlement; V_{L1} and V_{L2} are the ground loss ratio of the first tunnel construction and the additional ground loss ratio of the second tunnel construction, respectively; K_1 and K_2 are the settlement trough width coefficient of the first tunnel construction and the settlement trough width coefficient of the second tunnel construction, respectively; $Adj.R_1^2$ and $Adj.R_2^2$ are the adjustment coefficient of the first tunnel construction and the adjustment coefficient of the second tunnel construction, respectively (the closer the adjustment coefficient is to 1, the higher the fitting degree).

(1) Applicability analysis of Peck formula

The surface settlement caused by the first tunnel construction was fitted to obtain $Adj.R_1^2$ = 0.87~0.99 and an average of 0.97. The additional surface settlement caused by the second tunnel construction was fitted to obtain $Adj.R_2^2$ = 0.71~0.99 and an average of 0.89. It may be inferred that the Peck formula is applicable for analysing and forecasting surface settling induced by double-line tunnel construction in water-rich soft stratum.

(2) Analysis of settlement trough width coefficient

The settlement trough width coefficient is an empirical coefficient related to soil characteristics that should be analysed independently depending on the stratum combination. The width coefficient of the settlement trough K_1 = 0.44~0.49 for the first tunnel construction, with an average of 0.46; the width coefficient of the additional settlement trough K_1 = 0.48~0.53 for the second tunnel construction, with an average of 0.50 when the shield tunnel is constructed in the homogeneous soft stratum. The width coefficient of the settlement trough K_1 = 0.30~0.41 or the first tunnel construction, with an average of 0.35; the width coefficient of the additional settlement trough K_1 = 0.43~0.48 for the second tunnel construction, with an average of 0.46 when the shield tunnel is constructed in the upper-soft and lower-hard stratum. It may be deduced that the settlement trough width coefficient K under homogenous soft stratum is more than that under upper-soft and lower-hard stratum, and that the K of the second tunnel construction is bigger than that of the first tunnel construction. The increase in K is due to the disturbance of the stratum caused by the first tunnel construction.

(3) Analysis of ground loss ratio

The ground loss ratio is significantly related to the stratum condition and the construction level, so the data are of high discreteness. In general, the ground loss ratio V_{L1} = 0.54~1.20% for the first tunnel construction, with an average of 0.78%; the additional ground loss ratio V_{L2} = 0.38~1.67% for the second tunnel construction, with an average of 0.97%. It can be concluded that the additional ground loss ratio of the second tunnel construction is greater than that of the first tunnel construction. This is because of the stratum disturbance induced by the first tunnel building. On the other hand, the secondary disturbance caused by the second tunnel construction makes it more difficult to control the ground deformation.

(4) Analysis of surface settlement pattern

The midpoint of the double-line tunnel axes with the first tunnel for the negative direction, and the second tunnel for the positive direction was taken as the coordinate origin. The surface monitoring data and the corresponding fitting curves are shown in Figure 4, and the settlement duration curves are shown in Figure 5. The first tunnel's surface settlement was in the "single-groove" mode, with the maximum settlement right above the metro line's center and symmetrically distributed settlement troughs. In the shield portion, the clear distance of a double-line tunnel at each monitoring section was less than twice the tunnel diameter. The surface settlement of a double-line tunnel was in the "single-groove" mode, with the highest settlement on the side of the metro line with the most ground loss and asymmetrically distributed settlement troughs. Compared with the surface settlement of the first tunnel, the second tunnel changed the surface settlement trough model and increased the maximum settlement and the settlement trough width.

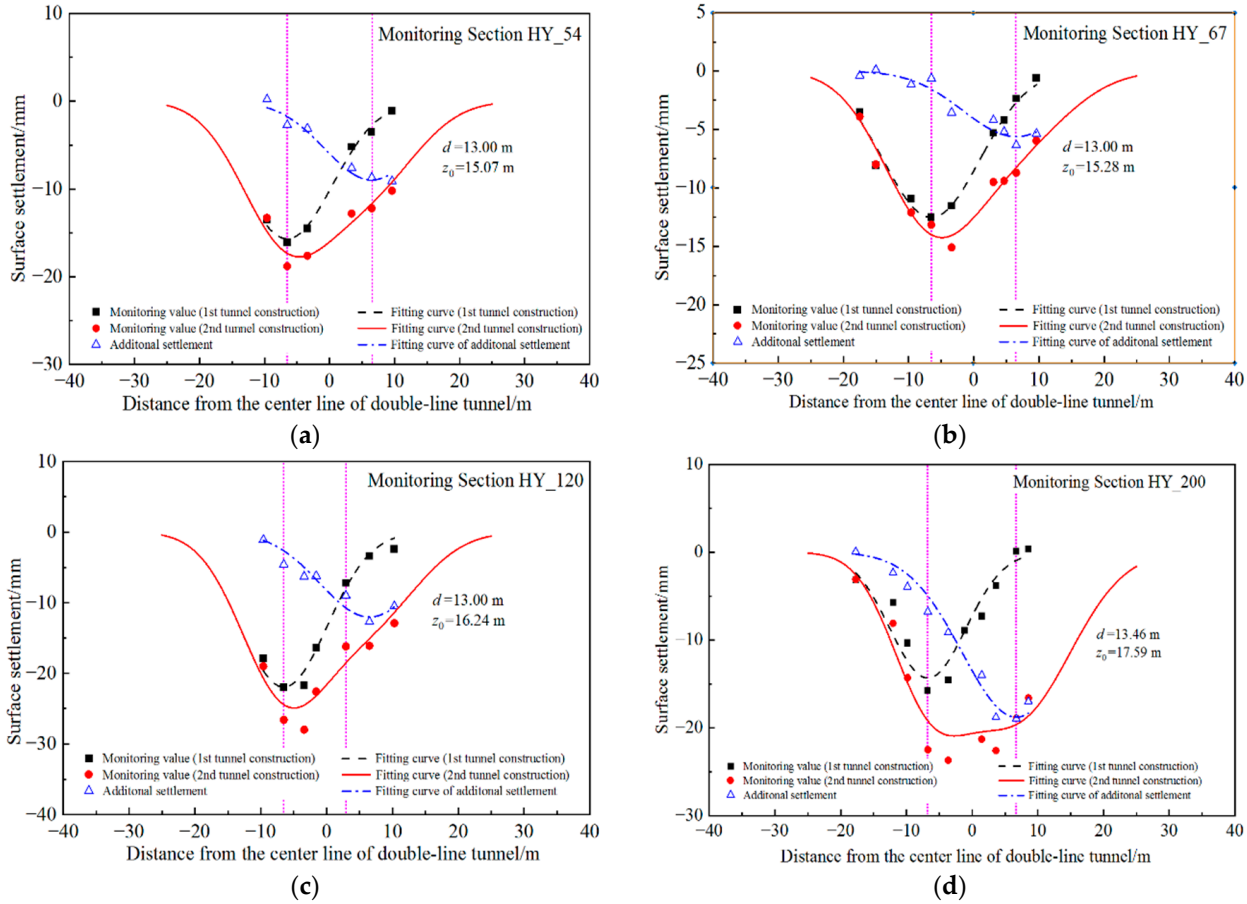

Figure 4. Settlement fitting curves of monitoring sections. (**a**) Monitoring section HY-54. (**b**) Monitoring section HY-67. (**c**) Monitoring section HY-120. (**d**) Monitoring section HY-200.

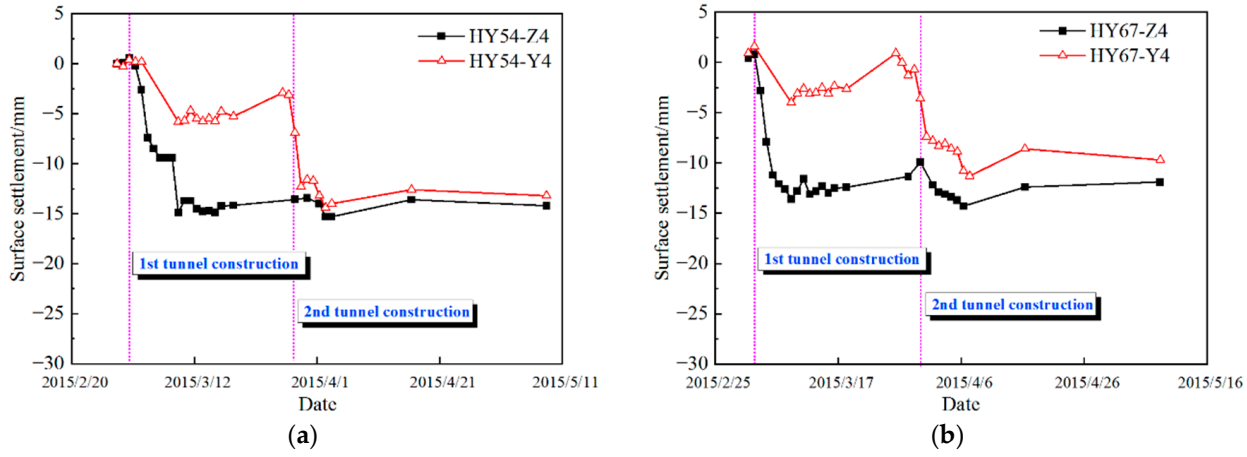

Figure 5. Settlement duration curves of monitoring sections. (**a**) Monitoring section HY-54. (**b**) Monitoring section HY-67.

The analysis of measured data showed that the maximum surface settlement S_{max} = −14.20~−28.00 mm after the double-line tunnel excavation, with an average of −20.73 mm. The influence of shield tunneling on surface settling in Tianjin's water-rich soft stratum could be inferred to be acceptable. The surface settlement of the water-rich soft stratum could be controlled within 20~30 mm by setting reasonable shield tunneling parameters.

4. Refined Numerical Simulation of Shield Tunneling

4.1. Numerical Model and Calculation Parameters

FLAC3D 6.0 software was used to develop a revised numerical model that can carry out the fluid–structure interaction analysis, as illustrated in Figure 6, to further examine the influence law of shield tunneling parameters on ground deformation in water-rich soft stratum. The numerical calculation model was set as length × height × width = 80 × 60 × 35 m, which was large enough to avoid the influence of boundary effects. The numerical model contained approximately 54,325 nodes and 50,560 three-dimensional elements. The tunnel's diameter was 6.2 m, with an overburden thickness of 10 m, and the groundwater level was located on the surface. The boundary conditions of the numerical model included two types: displacement boundary conditions and pore boundary conditions. Displacement boundary condition: normal displacement constraints were imposed on the side and bottom of the model. Pore boundary condition: hydrostatic pressure with a gradient of 10 kPa/m was imposed below the groundwater table on the side of the model, while the pore water pressure above the groundwater table was simplified to 0. The shield shell, lining, and tunnel face were set as impermeable boundaries. The support pressure of the excavation face was simulated by applying the surface load distributed along with the depth trapezoid on the excavation face. The jacking pressure on the segments was simulated by applying the element node force on the shield tail segment, and the ground deformation caused by the overcut was simulated by constructing a conical shield shell [20]. To approximate shield advancement, the stiffness transfer method was used [27]. The model advanced the length of one segment ring in each calculation cycle, with each cycle lasting for 4 h. The blue line and red dots in Figure 6 indicate the layout of the monitoring points. Measuring points A, B, C, and D were located on the surface, tunnel vault, bottom, and hance, respectively. The soil constitutive model was the Mohr-Coulomb model, and the equivalent zone constitutive model was the isotropic elastic model. The necessary parameters of the soil for the simulation calculation included the modulus of elasticity, Poisson's ratio, cohesion, internal friction angle, bulk density, void ratio, and permeability coefficient. The soil bulk density was obtained from geological exploration reports. The remaining parameters were obtained from the laboratory test. Table 2 shows the soil and equivalent zone calculation parameters. The equivalent zone was a treatment for the shield tail gap and the slurry filling in the gap that is equivalent.

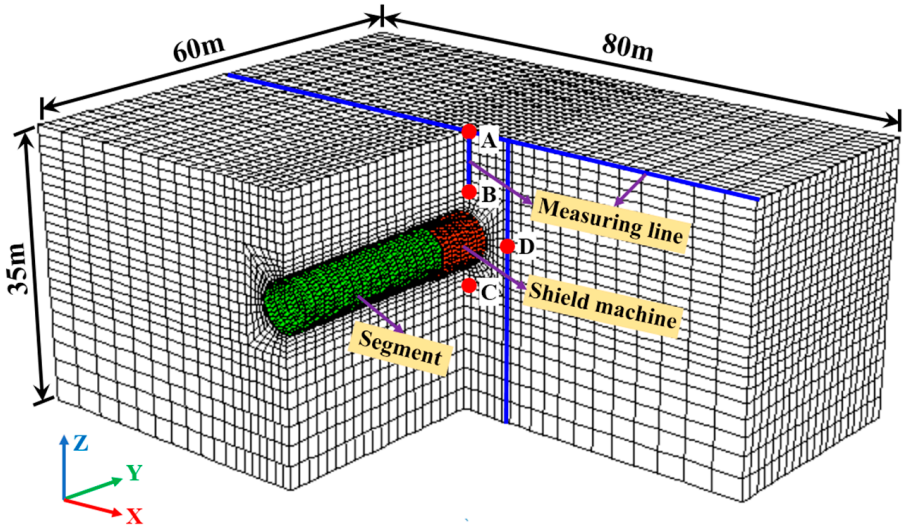

(**a**)

Figure 6. *Cont.*

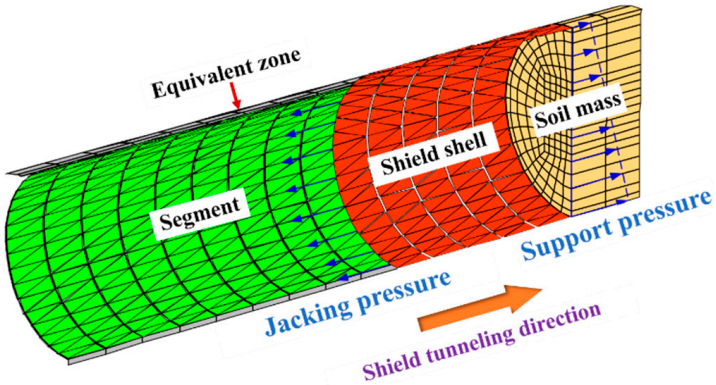

(**b**)

Figure 6. Numerical model of EPB shield. (**a**) Grid division diagram. (**b**) Local features of the model.

Table 2. Calculation parameters of soil and equivalent zone.

Layer	Modulus of Elasticity (MPa)	Poisson's Ratio	Cohesion (kPa)	Internal Friction Angle (°)	Bulk Density (kN/m^3)	Void Ratio	Permeability Coefficient (cm·s^{-1})
Upper silty clay	5.5	0.30	15.0	21.0	19.6	0.85	2.0×10^{-6}
Silt	11.0	0.25	7.8	33.0	19.9	0.65	4.0×10^{-5}
Lower clay silty	6.0	0.30	22.0	21.0	19.8	0.73	2.0×10^{-6}
Equivalent zone	50.0 (early stage) 500.0 (later stage)	0.30	/	/	21.0	0.85	1.0×10^{-6} (early stage) 1.0×10^{-9} (later stage)

The shield shell and segment were simulated by lining structural elements, and the constitutive model was the isotropic elastic model. Considering the segments as the homogeneous ring, the bending stiffness rate was introduced to simulate the influence of the joint on the segment stiffness. In the model, the bending stiffness rate of the segment was taken as 0.75 [28]. According to research results [20], the sliding friction coefficient between the shield skin and soil μ was 0.15~0.30 when the shield moved. The static friction coefficient between the shield skin and soil μ was 0.25~0.45, and the static friction coefficient between segment and grouting body μ was 0.30~0.40 as the shield started up. Therefore, the shield shell's shear coupling spring friction angle in the model was set to 7° (corresponding to μ = 0.17), while the segment's shear coupling spring friction angle was set to 17° (corresponding to μ = 0.31). The calculation parameters of the structural element are shown in Table 3.

Table 3. Calculation parameters of structural elements.

Item	Modulus of Elasticity (GPa)	Poisson's Ratio	Thickness (m)	Bulk Density (kN/m^3)	Normal Coupling Spring		Shear Coupling Spring		
					Rigidity (N·m^3)	Tensile Strength (Pa)	Rigidity (N·m^3)	Tensile Strength (Pa)	Cohesion (kPa)
Shield shell	210.0	0.20	0.20	78.5	1×10^9	0	1×10^9	9~15	0
Segment	25.9	0.20	0.35	25.0	1×10^9	0	1×10^9	17	0

4.2. Simulation of Interaction between Shield Skin and Soil

Due to the need for shield rectification and resistance reduction, the diameter of the cutter head is usually larger than the diameter of the shield tail, and the shield shell is a conical surface with a certain slope [20]. The soil around the shield shell will create

radial displacement pointing to the tunnel axis as the shield advances. In this paper, the node radial displacement was applied to the shield shell elements, and the surrounding soil elements were moved by the interaction between the lining elements and grid units to simulate the ground deformation caused by the overcut, as shown in Figure 7. The calculation correlation of radial displacement Δr was as follows:

$$\Delta r = \frac{L_r \times (D_e - d_e)}{2L_e} \quad (2)$$

where D_e is the diameter of the cutter head; d_e is the diameter of the shield tail; L_r is the length of the segment; L_e is the length of the shield shell. This paper set L_r = 1.5 m, $L_e = 5L_r$ = 7.5 m and Δr = 0.001 m.

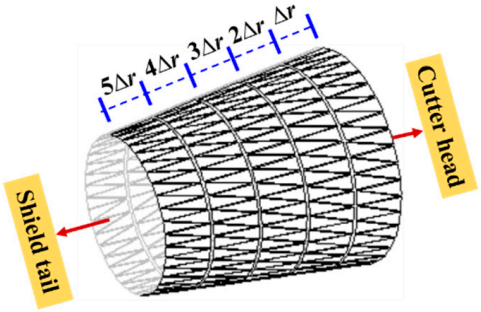

Figure 7. Conical shield shell (180-fold magnified).

The soil around the shield shell will create horizontal displacement pointing in the tunneling direction as the shield advances [29,30]. In the current study, the constant node velocity along the tunneling direction was applied to the shield shell elements with the interfacial shear coupling spring activated to simulate the friction between the shield skin and the soil. According to the interface characteristics of the lining elements (Figure 8), the simulation method could create friction related to the normal compressive stress of the interface and control the shield posture. As shown in Figure 9, the soil around the shield shell generated horizontal displacement under the action of friction, resulting in ground uplift in front of the excavation face and ground settlement behind the excavation face. The friction between the shield skin and soil could be controlled by changing the friction angle of the interface shear coupling spring.

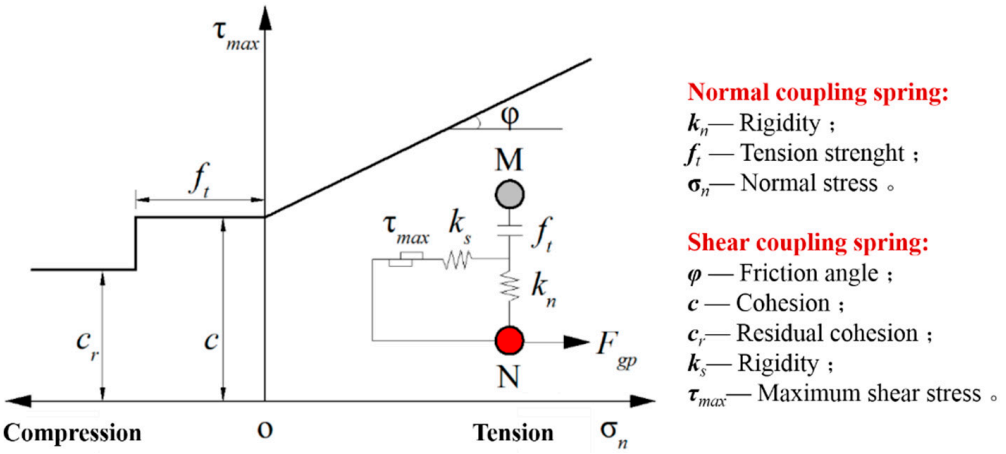

Figure 8. Interface behavior of liner structural elements.

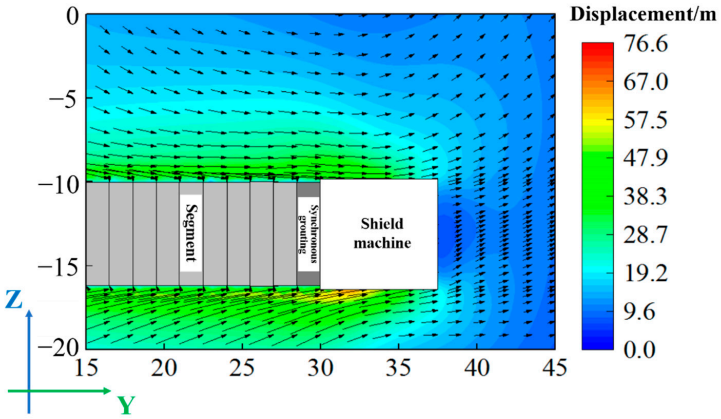

Figure 9. Displacement vector diagram in the longitudinal section.

4.3. Simulation of Synchronous Grouting

In synchronous grouting, the grouting pressure gradually decreases with slurry penetration and eventually stabilizes near the pore water pressure [31]. In the current study, the synchronous grouting process is simulated by applying a flux boundary to the equivalent zone element based on seepage–stress coupling theory, and the slurry hardening process is simulated by altering the elastic modulus of the equivalent zone element and the permeability coefficient. The pore water pressure and volume increment of the equivalent zone element indicate the synchronous grouting pressure and quantity, respectively. Variations in pore water pressure will alter volume strains in the fluid-structure interaction numerical simulation. Therefore, the constitutive equation for porous media in incremental form is as follows:

$$\Delta\sigma'_{ij} + \alpha\Delta p\delta_{ij} = H_{ij}(\sigma_{ij}, \Delta\varepsilon_{ij}) \tag{3}$$

where $\Delta\sigma'_{ij}$ is the effective stress increment; α is the Biot coefficient; Δp is the pore water pressure increment; δ_{ij} is the Kronecker delta; H_{ij} is the function related to the mechanical behavior of the medium; σ_{ij} is the total stress; $\Delta\varepsilon_{ij}$ is the total strain increment.

The pore water pressure of the equivalent zone and vertical displacement of monitoring point B are illustrated in Figure 10 for one excavation step of the shield passing through measuring point B. According to findings, in case the segments fall from the shield tail, the elastic modulus of the equivalent zone was taken as a minimum due to the shield-end structural spacing, and therefore the settlement of point B increased. The injection pressure in the shield tail gap gradually increased as the synchronous grouting progressed, and the elevation of point B increased accordingly. After completing synchronous grouting, the grouting pressure in the shield tail gap gradually decreased with a slight settlement at point B.

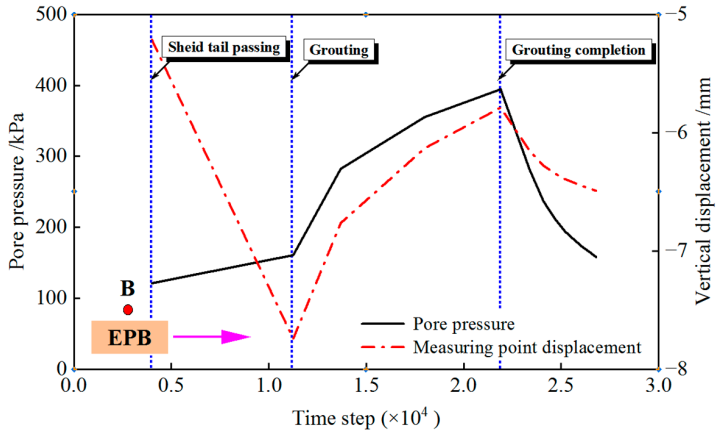

Figure 10. Grouting pressure and settlement at point B.

5. Model Validation

Based on previous research [20,30], ground deformation is mainly related to the key construction characteristics of shield tunneling, such as the support pressure at the excavation face, the friction between the shield skin and soil, and the quantity of synchronous pouring. In the first phase of the model validation process, nondimensional processing key elements are considered.

The support pressure ratio expresses the support pressure level, and its calculation correlation is:

$$P_s^* = p_s / \sigma_h \tag{4}$$

where p_s is the support pressure at the center of the excavation face; σ_h is the total horizontal stress at the center of the excavation face.

The friction coefficient expresses the friction level between the shield skin and soil, and its calculation correlation is:

$$F_f^* = 4F_f / \left[\pi D_e L_e \left(p_{e1} + p_{e2} + q_{e1} + q_{e2} + p_g\right)\right] \tag{5}$$

where F_f is the friction between the shield skin and soil; p_{e1} is the vertical earth pressure at the top of the shield; p_{e2} is the vertical earth pressure at the bottom of the shield; q_{e1} is the horizontal earth pressure at the top of the shield; q_{e2} is the horizontal earth pressure at the bottom of the shield; p_m is the earth counterforce.

The synchronous grouting ratio expresses the synchronous grouting quantity level, and its calculation correlation is:

$$V_g^* = V_g / V_{void} \tag{6}$$

where V_g is the synchronous grouting quantity within the length of one segment ring; V_{void} is the ground loss caused within the length of one segment ring.

To clarify the evolution characteristics of the ground settlement and excess pore water pressure during shield tunneling, the calculation condition ($P_s^* = 0.90$, $F_f^* = 0.38$, $V_g^* = 1.27$) is chosen to perform the simulation.

Figure 11 depicts the vertical displacement development curves of the monitoring points. According to the calculation results, the settlement value of point B was greater than that of point A before the shield passed through, which indicated that the soil in the monitoring zone was in a state of vertical expansion. When the shield passed, the uplifting of point B became evident due to the synchronous grouting impact. In addition, the changing trend of the vertical displacement of points C and B was basically the same; however, the direction was opposite.

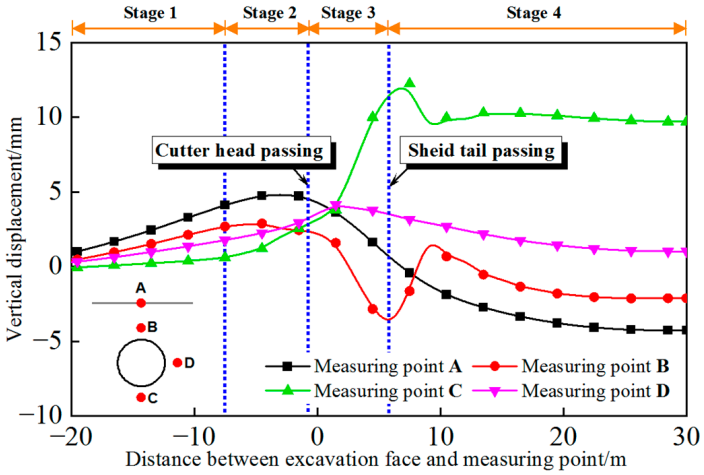

Figure 11. Settlement development curves at monitoring points.

The excess pore water pressure development curves at the monitoring points are shown in Figure 12. According to the findings, it can be concluded that the excess pore water pressure of the monitoring points was closely related to the shield tunneling, and the variations were consistent with the monitoring results in Shanghai [32] and Hangzhou [33].

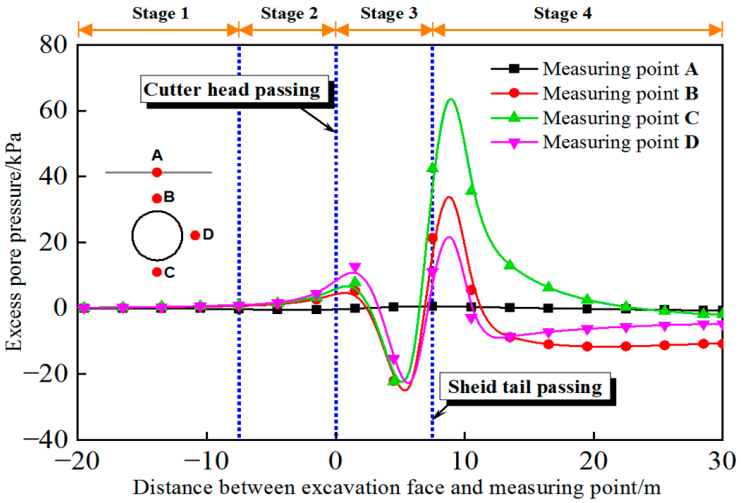

Figure 12. Excess pore water pressure development curves at monitoring points.

The ground settlement and pore water pressure responses caused by shield tunneling in water-rich soft stratum can be categorized into four phases. Stage 1: When the shield machine approaches, small ground deformation is observed. Stage 2: Sensible ground deformation and positive pore water pressure are induced by the arrival of the cutterhead. Stage 3: During the shield passage, the conical shield shell leads to ground loss and the pore water pressure at the measurement point decreases to a negative value. Stage 4: Pour water pressure increases from negative to positive values, and ground deformation rebounds, caused by tail void grouting. As the shield machine drives away, excess pore water pressure dissipates, and the ground settlement increases slightly.

In summation, the refined shield tunneling model developed in the current study can accurately simulate the vertical ground displacement variation law and excess pore water pressure induced by shield tunneling disturbance in water-rich soft stratum. Therefore, in the next section, the refined model was utilized to investigate the impact of shield tunneling parameters.

6. Influence Analysis of Construction Parameters and Field Verification

6.1. Impact Analysis of Support Pressure on Excavation Face

The calculation condition ($F_f^* = 0.38, V_g^* = 1.00, P_s^* = 0.70 \sim 1.10$) was selected to analyse the influence of the excavation face support pressure. Figure 13 depicts the vertical settlement curve for various P_s^* at point A. (Uplift is positive, and settlement is negative). According to the findings, it was concluded that with the increase in P_s^*, the uplift value of An increased when the cutter head passed through it, and the settlement value of A decreased when the shield tail passed through it. The reason behind this is that the support pressure maintains the layer's stability by improving the stress state of the stratum. Therefore, P_s^* only altered the vertical settlement of A rather than its settlement form. The vertical displacement of the soil above the shield is shown in Figure 14. The maximum value of the ground settlement was located at a certain distance above the shield, and synchronous grouting pressure lifted the soil near the vault. Figure 15 depicts the horizontal displacement along the axis direction at the tunnel's hance. As seen from the results, the horizontal displacement of the stratum along the axial direction indicated the tunnel excavation direction and the maximum displacement was detected at the lower side of the hance due to the friction between the shield skin and the soil. The horizontal displacement

along the transverse direction at the hance of the tunnel is presented in Figure 16. According to the findings, the transverse horizontal displacement of the stratum around the shield pointed to the stratum direction, while the transverse horizontal displacement of the stratum far away from the shield pointed to the tunnel direction, and the maximum value was detected at the hance, which was caused by synchronous grouting. The radial displacement of the segment is given in Figure 17. In engineering practice, ovality (the difference between the maximum and minimum diameter) is frequently employed to represent the degree of deformation of segments [24]. Figures 14–17 show that with the increase in P_s^*, the vertical displacement of the stratum above the shield gradually decreased; the horizontal displacement of the stratum on the side of the shield gradually increased; the ovality of the segment decreased from 17.42 mm to 17.13 mm, and the observed change was not obvious.

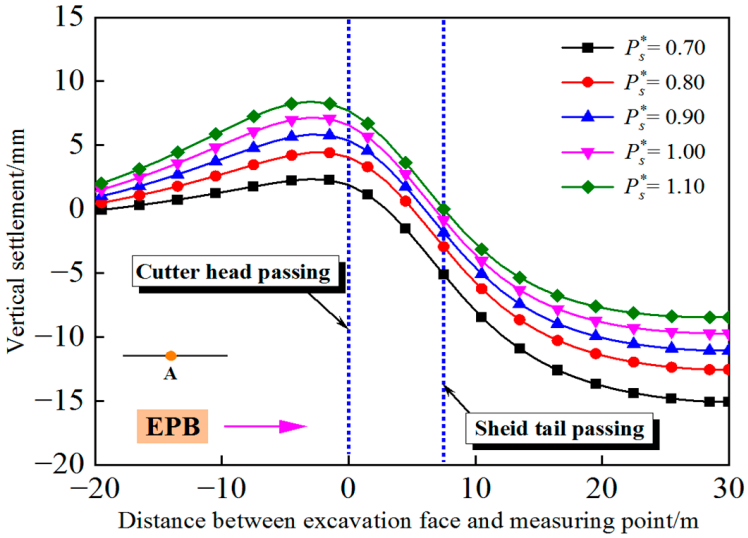

Figure 13. Vertical settlement at point A under different support pressure ratios P_s^*.

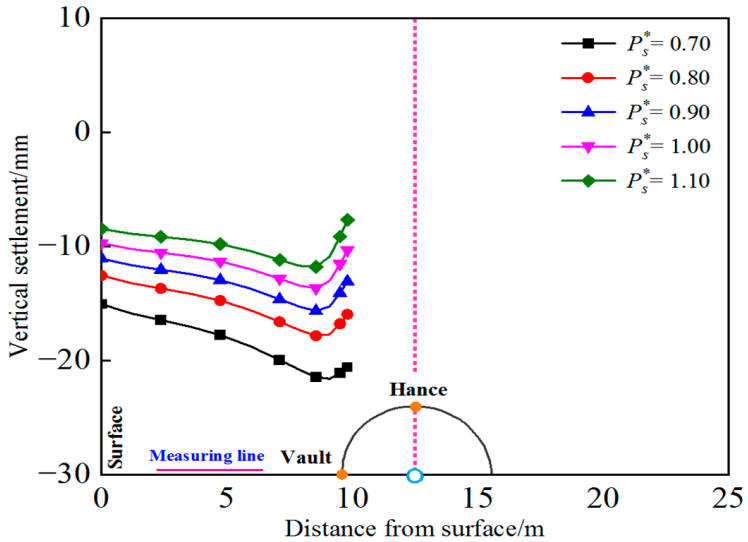

Figure 14. Vertical deformation of the stratum under different support pressure ratios P_s^*.

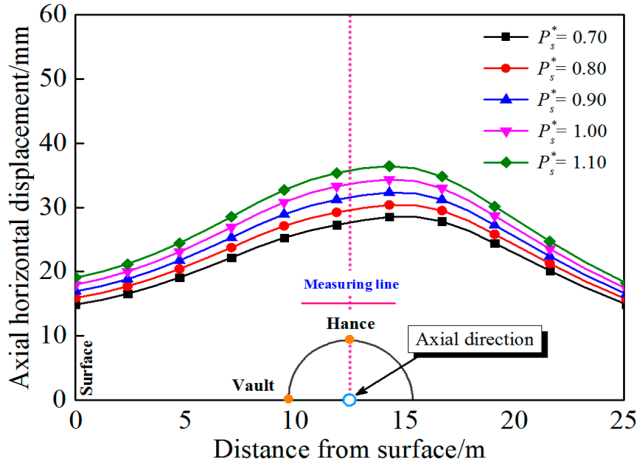

Figure 15. Horizontal deformation of the stratum along the axis direction under different support pressure ratios P_s^*.

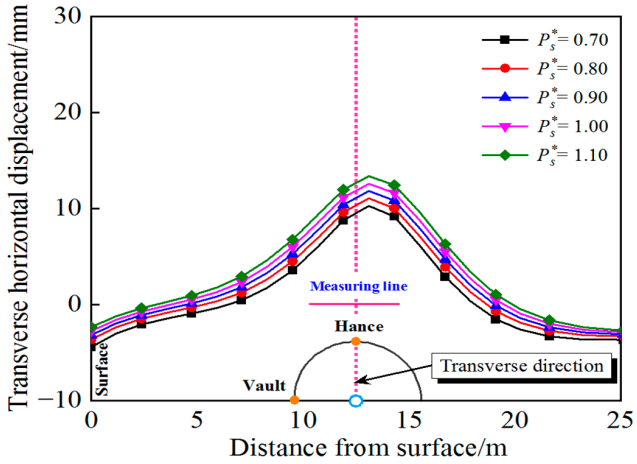

Figure 16. Horizontal deformation of the stratum along the transverse direction under different support pressure ratios P_s^*.

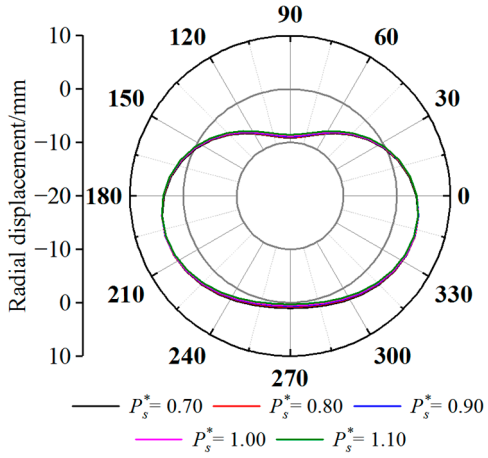

Figure 17. Lining ovality under different support pressure ratios P_s^*.

Therefore, increasing the support pressure is beneficial for controlling deformation in water-rich soft stratum. To conclude, the earth pressure should be strictly monitored in actual engineering, and an appropriate cutter head excavation rate and screw conveyor speed should be adjusted to preserve stratum stability.

6.2. Impact Analysis of Friction between Shield Skin and Soil

The calculation condition ($P_s^* = 0.90, V_g^* = 1.00, F_f^* = 0.13 \sim 0.68$) was selected to analyse the influence of the friction between the shield skin and soil. Figure 18 depicts the vertical settlement curve at point A for various F_f^*. It can be concluded that with the increase in F_f^*, the uplift value of An increased when the cutterhead passed through, and the settlement value of A also increased when the shield tail passed through. This was because the ground around the shield produced horizontal displacement under the friction between the shield skin and the soil, which indicated the direction of tunneling and compressed the front layer, causing elevation, and collapsed the layer after the shield passed. The vertical displacement of the soil above the shield is given in Figure 19. In addition, the horizontal displacements along the axial and transverse directions at the hance of the tunnel are presented in Figures 20 and 21, respectively. The radial displacement of the segment is shown in Figure 22. According to the results, it can be seen from Figures 19–22 that with the increase of F_f^*, the vertical displacement of the stratum above the shield gradually increased; the horizontal displacement of the stratum on the shield's side increased gradually; the ovality of the segment increased from 16.53 mm to 18.30 mm, and a notable change was not observed.

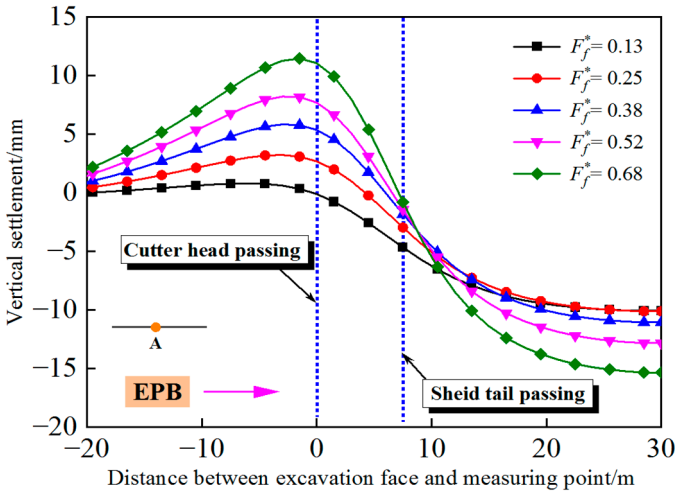

Figure 18. Vertical settlement at point A under different friction coefficients F_f^*.

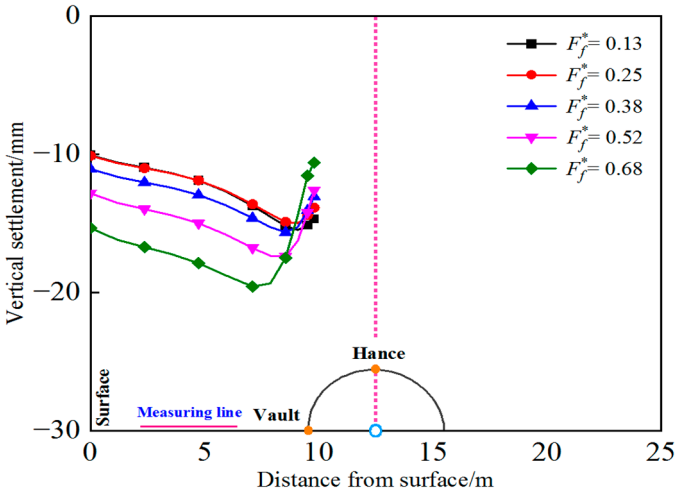

Figure 19. Vertical deformation of the stratum under different friction coefficients F_f^*.

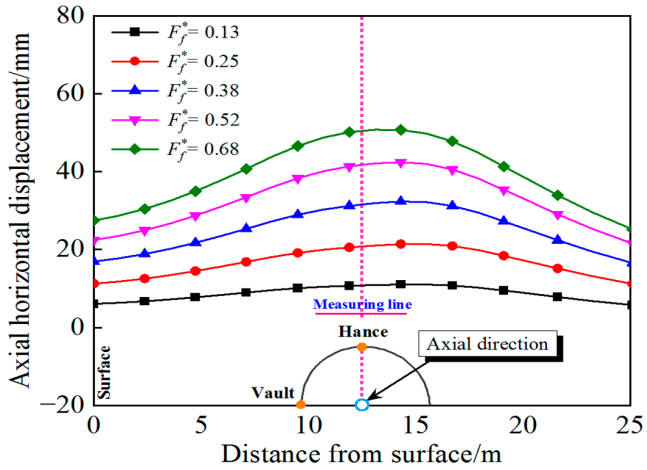

Figure 20. Horizontal deformation of the stratum along the axis direction under different friction coefficients F_f^*.

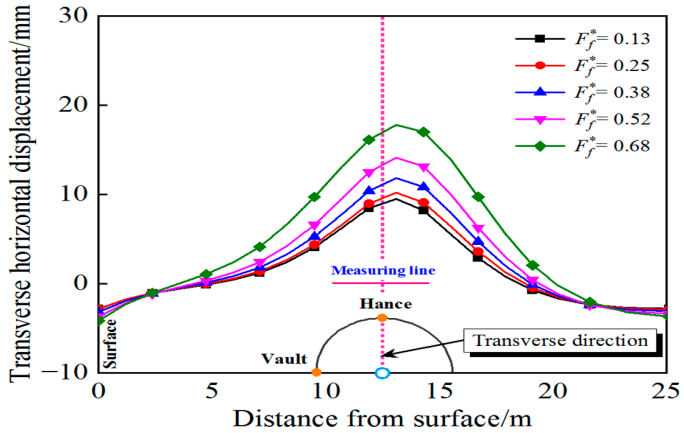

Figure 21. Horizontal deformation of the stratum along the transverse direction under different friction coefficients F_f^*.

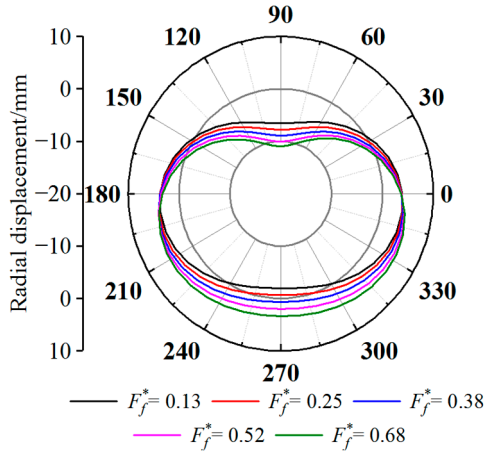

Figure 22. Lining ovality under different friction coefficients F_f^*.

Hence, increasing the friction between the shield skin and the soil was extremely detrimental to the deformation control of the water-rich soft stratum. Consequently, the jacking pressure should be closely monitored in practice, and bentonite slurry should be injected around the shield shell in time to reduce friction between the shield skin and the soil.

6.3. Impact Analysis of Synchronous Grouting Quantity

The influence of the synchronous grouting quantity was investigated based on the ($P_s^* = 0.90, F_f^* = 0.38, V_g^* = 0.95 \sim 1.47$) calculation condition. The vertical settlement curve at point A for different V_g^* values is given in Figure 23. According to the results, the influence of the V_g^* increment was reflected as the significant reduction of the settlement value of A when the shield tail passed through. The main reason for this situation is that the slurry after injection compensates for the ground loss by compacting the soil around the shield, which mainly affects the settlement value of the monitoring point. The vertical displacement of the soil above the shield is depicted in Figure 24. Figures 25 and 26 show the horizontal displacement in the axial and transverse directions at the hance of the tunnel, respectively. The radial displacement of the segment is shown in Figure 27. The following results were obtained with the examination of Figures 24–27: the vertical displacement of the stratum above the shield significantly decreased as V_g^* increased; the horizontal displacement of the stratum along the axial direction on the side of the shield gradually decreased, while the horizontal displacement along the transverse direction significantly increased, the ovality of the segment reduced from 18.21 mm to 13.83 mm, and the change was noticeable.

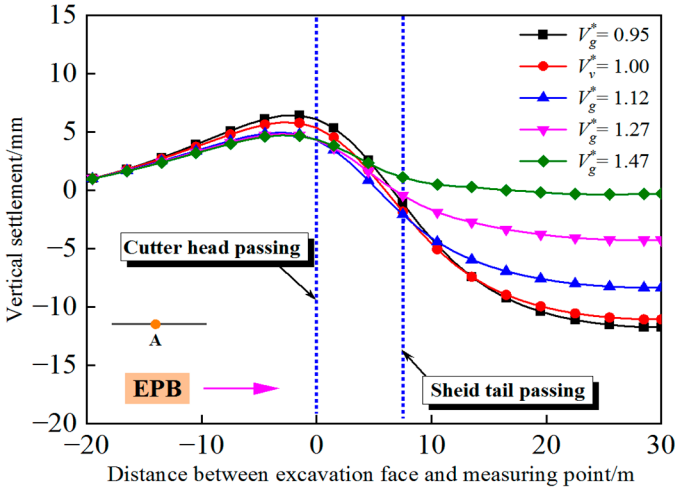

Figure 23. Vertical settlement at point A under different synchronous grouting ratios V_g^*.

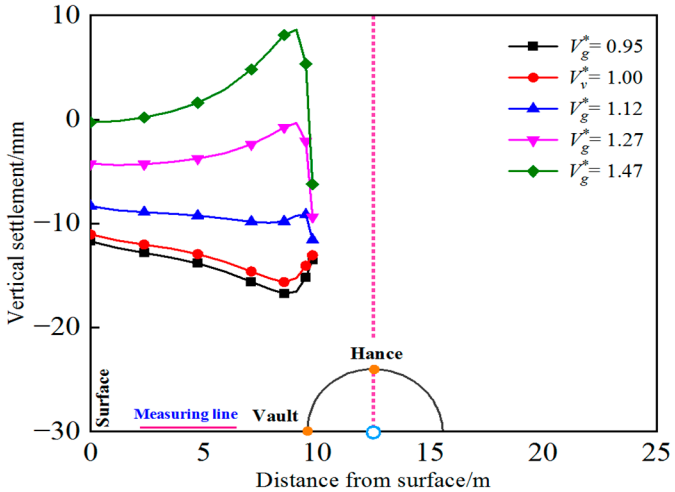

Figure 24. Vertical deformation of the stratum under different synchronous grouting ratios V_g^*.

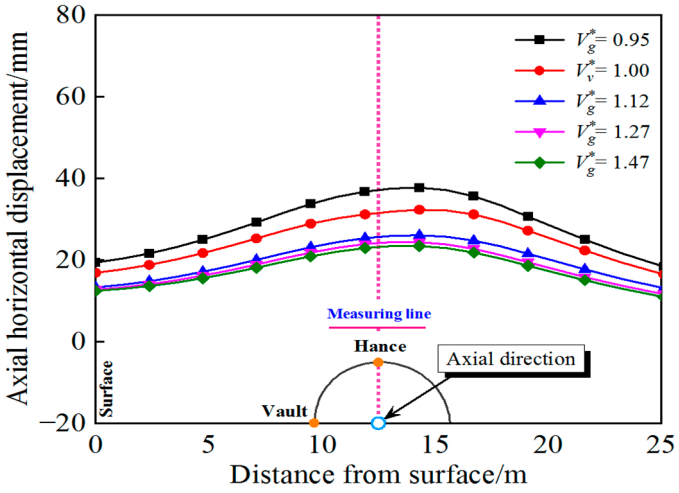

Figure 25. Horizontal deformation of the stratum along the axis direction under different synchronous grouting ratios V_g^*.

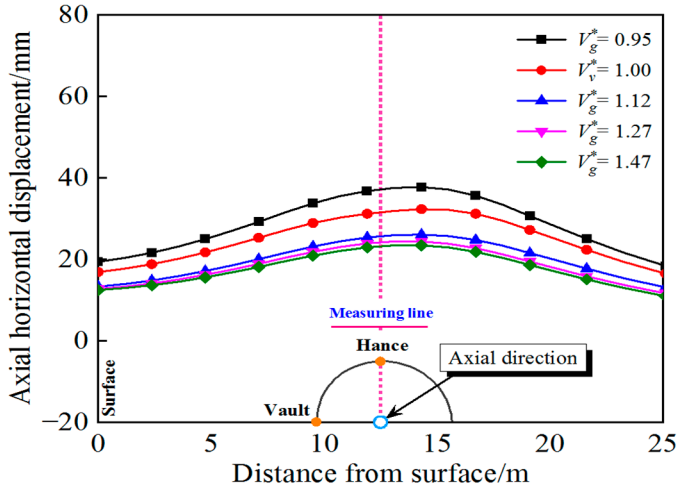

Figure 26. Horizontal deformation of the stratum along the transverse direction under different synchronous grouting ratios V_g^*.

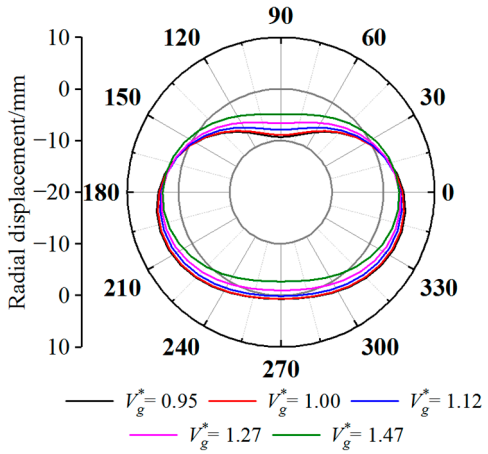

Figure 27. Lining ovality under different synchronous grouting ratios V_g^*.

As a result, increasing the amount of synchronous grouting helps control deformation in water-rich soft soil stratum. To minimize ground loss, the synchronous grouting operation should be completed on time and effectively in actual engineering.

To summarize, of the three contributing factors, the increase in friction between the shield skin and the soil was the most detrimental to the deformation control of the water-rich soft soil stratum. The friction between the shield skin and soil was related to the normal stress and interface friction coefficient acting on the periphery of the shield shell. Furthermore, the normal stress was related to the stress state of the stratum under shield tunneling disturbance, and the friction coefficient was influenced by the soil properties, shield shell surface roughness, and construction parameters. In actual engineering [29], timely injection of bentonite slurry can reduce the friction between shield skin and soil. Among the three influencing factors, the increase in synchronous grouting quantity was the most favorable to the deformation control of the water-rich soft soil stratum and segment. It exhibited a clear inhibitory influence on the segment's ovality and minimized the vertical and horizontal displacement of the stratum. In practice, timely and effective synchronous grouting can limit shield tunneling disruption to the stratum and segments.

6.4. Engineering Application Analysis

To verify the rationality of the refined numerical simulation method, the measured data of three monitoring sections were adopted for comparative analysis with the numerical simulation results. The monitoring segments were located on the surface above the segments, and the calculation parameters considered the average value of the parameters measured in the 10-segment distance range near the monitoring segments. Chamber pressure, synchronous grouting quantity, and jack pressure could be directly monitored in the process. Based on other scholars' achievement [29], the friction between shield skin and soil was adopted as 40% of the jack pressure. The measured and simulated values of TY-56 are shown in Figure 28. The simulated value of the chamber pressure was detected as 176 kPa ($P_s^* = 0.91$); the simulated value of the friction between the shield skin was measured as 4858 kN ($F_f^* = 0.33$); and the simulated value of the synchronous grouting quantity was 6.07 m^3 ($V_g^* = 0.33$). The measured and simulated surface settlements of TY-56 are presented in Figure 29. The measured values were found to be distributed near the simulated curves, indicating that the simulation results were essentially consistent with the measured results. Figure 30 depicts the measured and simulated values of segment ovality in monitoring section TY-56. According to the findings, good agreement between the simulated and measured values was revealed. Table 4 shows the measured and simulated maximum surface settlement and segment ovality for various monitoring sections. Table 4 shows that the minimum error between the measured values and the simulated values was 4% and the maximum error was 20%. The simulated values were in good agreement with the measured values, which indicated the suitability of the established numerical simulation method for the deformation character analysis caused by shield tunneling in water-rich soft stratum. In addition, the model was capable of calculation support for similar projects.

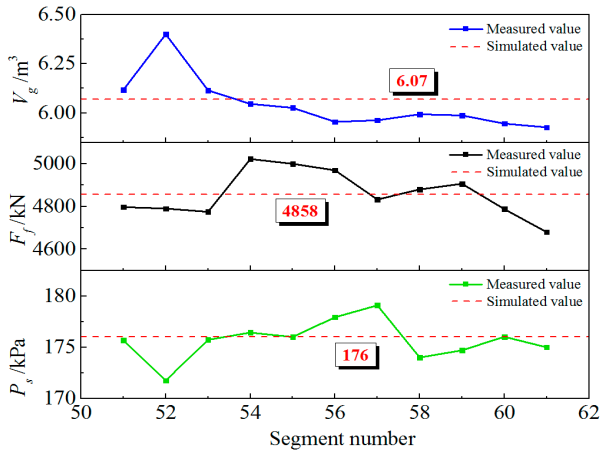

Figure 28. Excavation parameters at TY-56.

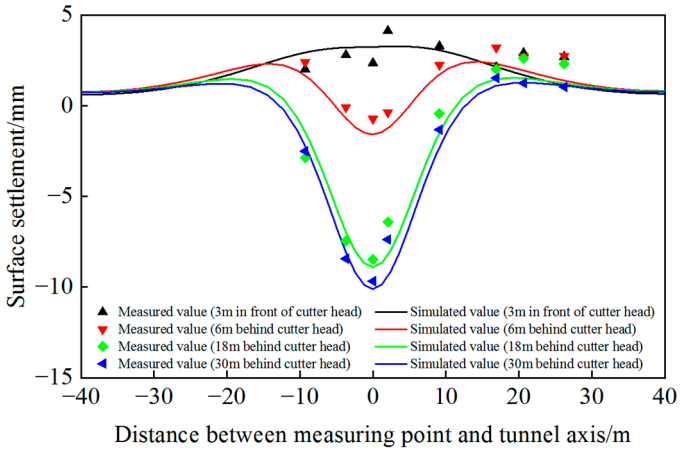

Figure 29. Surface settlement at TY-56.

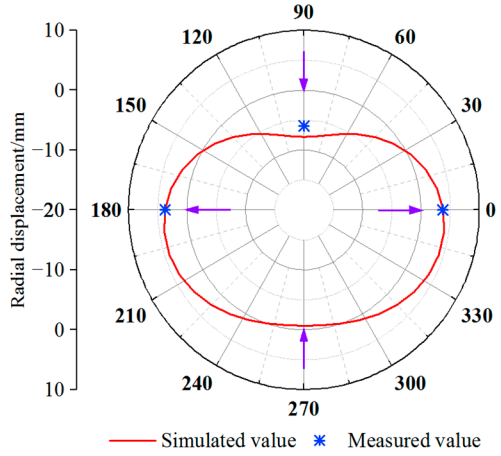

Figure 30. Lining ovality at TY-56.

Table 4. Comparison of the measured values and the simulated values at monitoring sections.

Monitoring Section	P_s^*	F_f^*	V_g^*	Maximum Surface Settlement (mm)			Lining Ovality		
				Measured Value	Calculated Value	Error	Measured Value	Calculated Value	Error
TY-56	0.91	0.33	1.01	−9.68	−10.11	4%	13.52	16.05	19%
TY-66	0.92	0.33	1.11	−5.04	−5.93	18%	12.21	14.71	20%
TY-290	1.20	0.45	0.99	−13.1	−12.46	5%	14.85	16.61	12%

6.5. Discussion

(1) In this study, the surface settlement of the water-rich soft stratum in Tianjin was fitted using the Peck formula. It should be noted that homogenous stratum is one of the application conditions for the Peck formula. The upper-soft and lower-hard stratum in this paper is treated as homogeneous stratum equivalently.

(2) In the current study, only a preliminary investigation of the ground deformation characteristics caused by the shield tunneling in water-rich soft stratum was carried out with a refined numerical model, where the hydraulic parameters were set as fixed values. In fact, the hydraulic parameters are related to the tunneling process and have obvious nonlinearity. Thus, it is thought that the research will pave the way for more in-depth studies.

(3) This paper did not consider the stratum damage caused by groundwater seepage, and a depth analysis related to the impact of non-homogeneous stratum on shield

tunneling in water-rich soft stratum was not carried out. Therefore, these contents can be regarded as fundamental for future research.

7. Conclusions

Field records and numerical analyses of the ground deformation induced by the process of shield tunneling in water-rich soft stratum were presented and discussed. With the proposed computational model, a parametric study was conducted to evaluate the influence of key construction elements of shield tunneling. The conclusions were as follows:

(1) According to data collected for Tianjin Metro Line 6, the surface settlement trough result was well fitted by a Gaussian distribution curve. The surface settlement ranges from −14.20 mm to −28.00 mm in Tianjin's water-rich soft stratum, which is at an acceptable level of engineering.

(2) A refined 3D model addressing fluid–structure interactions is developed to consider the construction process in water-rich soft stratum, including tunnel face advance, tail void grouting, lining installation, and grout hardening. The monitoring data of Tianjin Metro Line 6 are compared with the simulation results. The minimum error between the measured values and the simulated values was detected as 4% and the maximum error was detected as 20%. The simulation findings are in good agreement with the measured data, demonstrating the rationality and application of the refined numerical simulation method proposed in this paper for shield tunneling analysis in water-rich soft stratum.

(3) The impact of shield driving parameters on ground deformation is drawn from the parametric study. The friction between the shield skin and the soil is the most disadvantageous parameter for the deformation control among the three parameters studied in this paper. The increase in this parameter causes four adverse results: stratum uplift in front of the cutterhead; stratum settlement behind the shield tail; increase in horizontal displacement of the stratum along both the axial and lateral directions of the tunnel; and an increase in elliptical deformation of the segment ring. The synchronous grouting quantity is the most advantageous of the three parameters for deformation control. The increase in this parameter can reduce the settlement and the horizontal displacement along the axial direction of the tunnel while significantly reducing the elliptical deformation of the segment ring. In practical engineering, timely injection of bentonite slurry reduces friction between the shield skin and the soil, and effective synchronous grouting reduces ground loss.

Author Contributions: Conceptualization, X.L. and D.Z.; data curation, X.L.; funding acquisition, D.Z.; investigation, Y.H.; methodology, X.L.; project administration, D.Z.; software, X.L.; supervision, D.Z.; validation, X.L.; writing—original draft, X.L.; writing—review & editing, X.L. All authors have read and agreed to the published version of the manuscript.

Funding: This research was funded by Chinese National Natural Science Foundation, grant number 51738002 and National Key Research and Development Programs of China, grant number 2017YFC0805401.

Conflicts of Interest: The authors declare no conflict of interest.

References

1. Cao, L.Q.; Fang, Q.; Zhang, D.L.; Chen, T. Subway station construction using combined shield and shallow tunnelling method: Case study of Gaojiayuan station in Beijing. *Tunn. Undergr. Space Technol.* **2018**, *82*, 627–635. [CrossRef]
2. Zhang, Z.G.; Huang, M.S.; Pan, Y.T.; Jiang, K.; Li, Z.; Ma, S.; Zhang, Y. Analytical prediction of time-dependent behavior for tunneling-induced ground movements and stresses subjected to surcharge loading based on rheological mechanics. *Comput. Geotech.* **2021**, *129*, 103858. [CrossRef]
3. Liang, Y.; Chen, X.Y.; Yang, J.S.; Zhang, J.; Huang, L. Analysis of ground collapse caused by shield tunnelling and the evaluation of the reinforcement effect on a sand stratum. *Eng. Fail. Anal.* **2020**, *115*, 104616. [CrossRef]
4. Fang, Q.; Du, J.M.; Li, J.Y.; Zhang, D.L.; Cao, L.Q. Settlement characteristics of large-diameter shield excavation below existing subway in close vicinity. *J. Cent. South Univ.* **2021**, *28*, 882–897. [CrossRef]

5. Lin, X.T.; Chen, R.P.; Wu, H.N.; Cheng, H.Z. Deformation behaviors of existing tunnels caused by shield tunneling undercrossing with oblique angle. *Tunn. Undergr. Space Technol.* **2019**, *89*, 78–90. [CrossRef]
6. Lin, C.G.; Huang, M.S.; Nadim, F.; Liu, Z.; Yu, J. Analytical solutions for tunnelling-induced response of two overlying pipelines. *Tunn. Undergr. Space Technol.* **2021**, *108*, 103678. [CrossRef]
7. Li, X.Y. Water-Induced Disaster Mechanism and Safety Risk Control for Shield Tunnel Construction. Ph.D. Thesis, Beijing Jiaotong University, Beijing, China, 2019.
8. Peck, R.B. Deep Excavations and Tunneling in Soft Ground. In Proceedings of the 7th International Conference on Soil Mechanics and Foundation Engineering, Mexico City, Mexico, 29 August 1969; pp. 225–290.
9. Reilly, O.; New, W. Analysis of undrained soil for tunnelling-induced ground movements in clays. *J. Geotech. Geoenviron. Eng.* **1993**, *13*, 165–183.
10. Clough, G.; Schimidt, J. Investigation of deformation and collapse behavior of circular lined tunnels in centrifuge model tests. *Can. Geotech. J.* **1992**, *29*, 929–940.
11. Chen, C.S.; Xia, Y.Y. Adaptability study of Peck formula applied to shield tunneling in the area of the first grade terrace of the Changjiang river. *J. Wuhan Univ. Technol.* **2013**, *35*, 85–90.
12. Fang, Q.; Wang, G.; Yu, F.; Du, J. Analytical algorithm for longitudinal deformation profile of a deep tunnel. *J. Rock Mech. Geotech. Eng.* **2021**, *13*, 845–854. [CrossRef]
13. Sagaseta, C. Analysis of undrained soil deformation due to ground loss. *Geotechnique* **1987**, *37*, 301–320. [CrossRef]
14. Loganathan, N.; Poulos, H.G.; Xu, K.J. Ground and pile-group responses due to tunnelling. *Soils Found.* **2001**, *41*, 57–67. [CrossRef]
15. Pinto, F.; Zymnis, D.M.; Whittle, A.J. Ground movements due to shallow tunnels in soft ground. II: Analytical interpretation and prediction. *J. Geotech. Geoenviron Eng.* **2014**, *140*, 80–90. [CrossRef]
16. Atkinson, J.H.; Potts, D.M. Subsidence above shallow tunnels in soft ground. *J. Geotech. Eng. Div.* **1977**, *103*, 307–325. [CrossRef]
17. Chapman, D.N.; Ahn, S.K.; Hunt, D.V. Investigating ground movements caused by the construction of multiple tunnels in soft ground using laboratory model tests. *Can. Geotech. J.* **2007**, *44*, 631–643. [CrossRef]
18. Fang, Y.; Chen, Z.T.; Tao, L.M.; Cui, J.; Yan, Q. Model tests on longitudinal surface settlement caused by shield tunnelling in sandy soil. *Sustain. Cities Soc.* **2019**, *47*, 101504. [CrossRef]
19. Zhou, M.Z.; Fang, Q.; Peng, C. A mortar segment-to-segment contact method for stabilized total-Lagrangian smoothed particle hydrodynamics. *Appl. Math. Model.* **2022**, *107*, 20–38. [CrossRef]
20. Kasper, T.; Meschke, G. A 3D finite element simulation model for TBM tunnelling in soft ground. *Int. J. Numer. Anal. Methods Geomech.* **2004**, *28*, 1441–1460. [CrossRef]
21. Kasper, T.; Meschke, G. On the influence of face pressure, grouting pressure and TBM design in soft ground tunneling. *Tunn. Undergr. Space Technol.* **2006**, *21*, 160–171. [CrossRef]
22. Nagel, F.; Stascheit, J.; Meschke, G.; Koch, C.; Hegemann, F.; König, M. Process-oriented numerical simulation of mechanised tunnelling. In *Proceedings of the Technology Innovations in Underground Construction*; Beer, G., Ed.; Taylor and Francis: London, UK, 2009; Volume 87–127, pp. 111–152.
23. Nagel, F.; Stascheit, J.; Meschke, G. Process-oriented numerical simulation of shield-supported tunnelling in soft soils. *Geomech. Tunn.* **2010**, *3*, 268–282. [CrossRef]
24. Shi, J.K.; Wang, F.; Zhang, D.M.; Huang, H. Refined 3D modelling of spatial-temporal distribution of excess pore water pressure induced by large diameter slurry shield tunneling. *Comput. Geotech.* **2021**, *137*, 104312. [CrossRef]
25. Zheng, G.; Lu, P.; Diao, Y. Advance speed-based parametric study of greenfield deformation induced by EPBM tunneling in soft ground. *Comput. Geotech.* **2015**, *65*, 220–232. [CrossRef]
26. Attewell, P.B. Predicting the dynamics of ground settlement and its derivatives caused by tunnelling in soil. *Ground Eng.* **1982**, *15*, 13–22.
27. Wang, M.Q.; Chen, S.H. 3-dimensional non-linear finite element simulation of tunnel structure for moving-forward shield. *Chin. J. Rock Mech. Eng.* **2002**, *21*, 228–232. [CrossRef]
28. Huang, H.W.; Ling, X.U.; Yan, J.L.; Yu, Z.K. Study on transverse effective rigidity ratio of shield tunnels. *Chin. J. Geotech. Eng.* **2006**, *28*, 11–18.
29. Zhang, H.B. Numerical Simulation of the Influence of Shield Tunneling on Surrounding Environment. Ph.D. Thesis, Hehai University, Nanjing, China, 2005.
30. Lu, P. A Fuzzy Theory-Based Study on the Influence of Driving Parameters to the Surrounding Soil Deformation in Shield Tunneling. Ph.D. Thesis, Tianjin University, Tianjin, China, 2014.
31. Zhang, S.S.; Dai, Z.R.; Bai, Y. Research on the Dissipation Law of Grout Pressure during the Simultaneous Grouting of Shield Tunnel. *China Railw. Sci.* **2012**, *33*, 40–48.
32. Xiao, L.; Zhang, Q.H.; Zhu, J.W.; Yao, H. Study on the excess pore water pressure caused by shield tunneling. *Chin. J. Undergr. Space Eng.* **2010**, *6*, 1039–1043+1087.
33. Yu, X.F.; Ren, H.; Hu, X.D. Analysis of the disturbance to surrounding soils during shield driving for the hangzhou metro line. *Mod. Tunn. Technol.* **2014**, *51*, 166–173.